Supplementary Information

The Ginger-shaped Asteroid 4179 Toutatis: New Observations from a Successful Flyby of Chang'e-2

Jiangchuan Huang[1,3*], Jianghui Ji[2*], Peijian Ye[1], Xiaolei Wang[4], Jun Yan[5], Linzhi Meng[3], Su Wang[2], Chunlai Li[5], Yuan Li[6], Dong Qiao[7], Wei Zhao[8], Yuhui Zhao[2], Tingxin Zhang[1], Peng Liu[8], Yun Jiang[2], Wei Rao[3], Sheng Li[9], Changning Huang[10], Wing-Huen Ip[6,11], Shoucun Hu[2], Menghua Zhu[6], Liangliang Yu[2], Yongliao Zou[5], Xianglong Tang[8], Jianyang Li[12], Haibin Zhao[2], Hao Huang[3], Xiaojun Jiang[5], & Jinming Bai[13]

[1]China Academy of Space Technology, Beijing 100094, China.

[2]Key Laboratory of Planetary Sciences, Purple Mountain Observatory, Chinese Academy of Sciences, Nanjing 210008, China.

[3]Institute of Space System Engineering, Beijing 100094, China.

[4]Beijing Institute of Control Engineering, Beijing 100190, China.

[5]National Astronomical Observatories, Chinese Academy of Sciences, Beijing 100012, China.

[6]Space Science Institute, Macau University of Science and Technology, Taipa, Macau.

[7]Beijing Institute of Technology, Beijing 100081, China.

[8]Harbin Institute of Technology, Harbin 150001, China.

[9]School of Electronic Engineering and Computer Science, Peking University, Beijing 100871, China.

[10]Beijing Institute Of Space Mechanics and Electricity, Beijing 100076, China.

[11]Institute of Astronomy, National Central University, Taoyuan, Taiwan.

[12]Planetary Science Institute, AZ 85719, USA.

[13]Yunnan Astronomical Observatory, Chinese Academy of Sciences, Kunming 650011, China.

* The authors contribute equally to this work. To whom correspondence should be addressed. E-mail:jijh@pmo.ac.cn

1 Determination of imaging resolution

Considering Chang'e-2's characteristics of high control accuracy of attitude and orbit, wide FOV (field of view) of the imaging camera, and unavailable accuracy of orbital ranging data, a close-approach flyby strategy was designed specifically[36] to be well applicable to an approaching flyby mission with a high and stable relative velocity. The imaging scheme could reliably ensure the coverage of Toutatis in the FOV, as shown in Supplementary Figure 1.

As long as the closest-approach distance **L** is sufficiently small (actually approximately 770 m from Toutatis' surface), the resolution of some initial sequence of images with relatively large sizes can be kept high to calculate the parameters for the flyby. Once it entered the FOV in Image 1 (see Ref. [1] in the main text) in the figure, the asteroid Toutatis remained in the FOV, but its image size decreased as the departure distance grew. The camera optical axis pointed in the direction of the relative velocity between the probe and Toutatis. As shown in Supplementary Figure 1, Images 2 and 3 were used to calculate the variation in the flyby, where Δt denotes the time interval between two sequential images. By measuring images, solving geometric relations, and processing data, the approach distance **L**, imaging distance **S**, and resolution of each image could be determined for the Chang'e-2 observations (Ref. [1]).

2 Shape and Orientation

Several methods have been used to attempt to directly establish the 3-D model of the surface layer of Toutatis based on the optical images acquired by Chang'e-2. However, no satisfactory outcome was achieved because of the very narrow viewing-angle coverage of the optical images throughout the imaging process. Therefore, 3-D models developed based on delay-Doppler radar measurements were adopted to discern the attitude of Toutatis in the approaching epoch.

The attitude of a rigid body in space is determined by its rotations around three axes of an

orthogonal coordinate system. To define the attitude of Toutatis in each optical image (Supplementary Figure 2a), the three axes l_1, l_2, and l_3 were defined as follows: l_1 and l_2 extend through Toutatis' centroid along the directions of the long axis and short axis in the images, respectively, and they are perpendicular to each other. Furthermore, l_3 is perpendicular to the imaging plane and constitutes a right-handed coordinate system with l_1 and l_2.

The view direction and azimuth angle of the camera were used to determine an inertial coordinate system based on the attitude of the probe and its camera and the relative positions of Toutatis and Chang'e-2. First, we rotated the model of Busch et al. in intervals of 5° for each Euler angle around the three axes of the body-fixed coordinate system in space to match its shape to the optical images. We then chose three features of each optical image to ensure that it agreed well with the optical result from the view direction of Chang'e-2: the orientation of the asteroid's long-axis, the ratio of length to width, and the remarkable topographical feature at the joint of the two lobes of Toutatis. The aforementioned three features could be determined by rotating about l_1, l_2, and l_3, respectively.

The most approximate attitude was finally obtained by rotating the radar model and comparing it with the optical image, as shown in Supplementary Figure 2b. The coordinate transformation from the asteroid's body-fixed system to the J2000.0 equatorial coordinate system could then be expressed using three components of Euler angles as follows:

$$\vec{r} = R_z(12^\circ)R_x(-50^\circ)R_z(-32^\circ)\vec{R}, \tag{1}$$

where R_x and R_z are the standard rotation matrices for right-handed rotations around the X and Z axes, respectively. The direction of the principle axis was then obtained according to the attitude of the radar model, which is $(250 \pm 5^\circ, 63 \pm 5^\circ)$ in the J2000 ecliptic coordinate system. Corresponding errors may arise from the matching process and the comparisons with the results of delay-Doppler radar measurements.

3 Physical size analysis for Toutatis

TThe imaging strategy of infinite-point-staring,[36] which was specially designed for Chang'e-2 because the detector's principle axis pointed in the direction of the relative speed of the probe and Toutatis, provides a dedicated method of size resolution with multi-frame optical images. The detailed procedures are as follows: (1) contour extraction, line measurement, endpoint determination, and estimation of the point at infinity are implemented. (2) The parameters — field of view, sizes of image pixels, distances of imaging and flyby, etc. — that are involved in calculating the distances between length endpoints and the principal point of the CMOS detector are determined. (3) The coordinates of the length endpoints are obtained, and the length values are calculated. (4) The width value is calculated.

The size was statistically measured in the imaging space of the CMOS detector based on the illuminated region of Toutatis' surface. The mean Grubbs criterion was used to reject outliers during the process. A length and width of (4.75 $\times$ 1.95 km) $\pm 10\%$ are considered to be the best estimation of the actual size of Toutatis.

Because the size analysis is based on the regularity of the imaging sequence, the resolution is a more convenient and more practical method for measuring a physical size than is the scale description. As is well known, resolution is inversely proportional to imaging distance. For the first image out of the shadow of the probe panel, the resolution is 8.3 meters per pixel. The elongation of the physical size of an object in the image, which corresponds primarily to the asteroid's attitude in space, is 0.71$\pm$0.03. For the computation of the imaging distance, one can refer to Supplementary Section 1.

The physical scale of $\vec{R_a} = (4.60, 1.92)^{\mathrm{T}}$ from the radar model of Hudson et al. (see Ref. [5]) and the measuring size of $\vec{R_o} = (4.75, 1.95)^{\mathrm{T}}$ derived from the optical images are consistent with one another, as observed from the high similarity of the numerical values, the

highly positive covariance of $\rho = \left(\vec{R_a}^{\,\mathrm{T}} \cdot \vec{R_o}\right) / \left(\sqrt{\vec{R_a}^{\,\mathrm{T}} \cdot \vec{R_a}} \times \sqrt{\vec{R_o}^{\,\mathrm{T}} \cdot \vec{R_o}}\right) = 0.99998 \simeq 1$, and the comparable length-to-width ratios of 2.396 for $\vec{R_a}$ and 2.436 for $\vec{R_o}$.

4 Size-frequency Relationship

4.1 R-plot

The relative-plot (henceforth R-plot) method, which shows the crater size-frequency distribution for a body, was applied for Toutatis (see Figure 3 in the main text). The R-plot method was devised by the Crater Analysis Techniques Working Group[37] to better illustrate the size distributions of craters and crater number densities for determining the relative ages of various bodies.

The equation for the R value is

$$R = D^3 N / A(b_2 - b_1), \tag{2}$$

where D is the geometric mean diameter of size bin ($\sqrt{[b_1 b_2]}$), N is the number of craters in the size bin, A is the area over which the counts are acquired, and b_1 and b_2 are the lower and upper limits of the size bin, respectively. Usually, the size bins are in increments of $\sqrt{2}$ because there are many more small craters than large craters.[37,38] In this work, $\sqrt{2}$ was used as the size-bin increment for the R-plot. The error bars were determined as follows:

$$\pm\sigma = R/\sqrt{N}, \tag{3}$$

where R is the R value. In an R-plot, $\log(R)$ is plotted on the y axis, and $\log(D)$ is plotted on the x axis.

4.2 CSFD

The Cumulative Size-Frequency Distribution (CSFD) is typically used to determine absolute model ages for a geological unit. Here, we simply display the size distribution of the craters

rather than estimate the absolute model age. The x axis represents the crater diameter, and the y axis represents the number of craters that are larger than the corresponding diameter in the investigated area. The CSFD provides a simple method of expressing how the crater-size distribution changes as the crater diameter increases.

References

[36] Huang, J. C. et al. The approaching strategy and imaging design for (4179) Toutatis flyby mission of Chang'e-2. *Science China Technological Sciences* **43**, 478 (2013).

[37] Arvidson, R. E. Standard techniques for presentation and analysis of crater size-frequency data. *Icarus* **37**, 467 (1979).

[38] Strom, R. G. et al. The Origin of Planetary Impactors in the Inner Solar System. *Science* **309**, 1847 (2005).

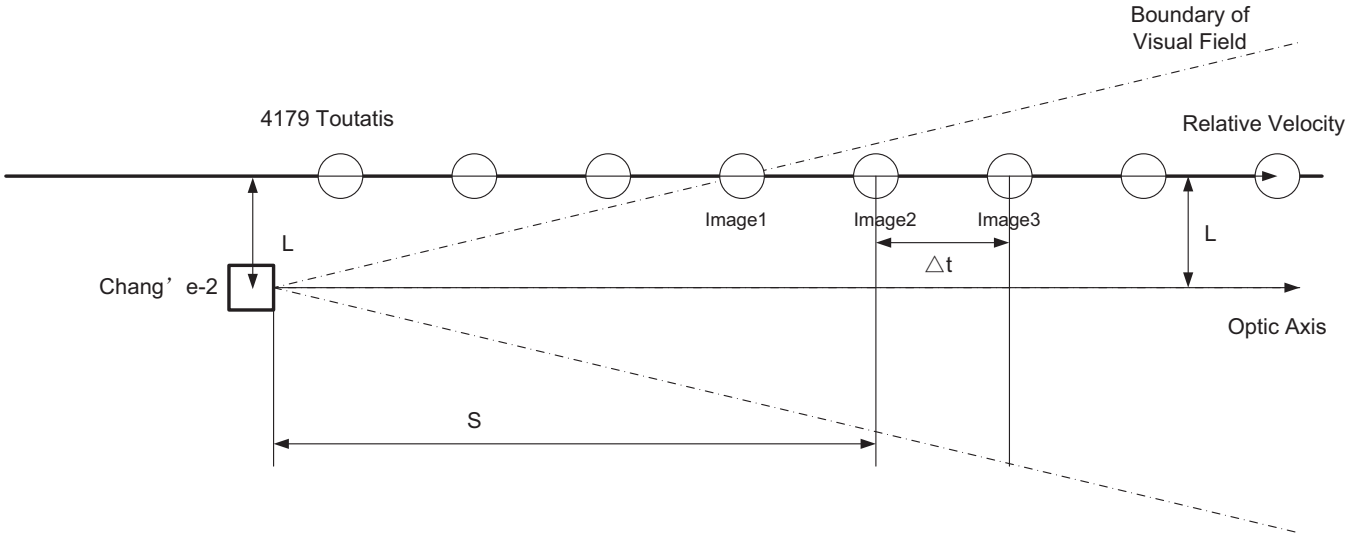

Figure 1 The geometry of the Chang’e-2 and Toutatis during the flyby epoch.

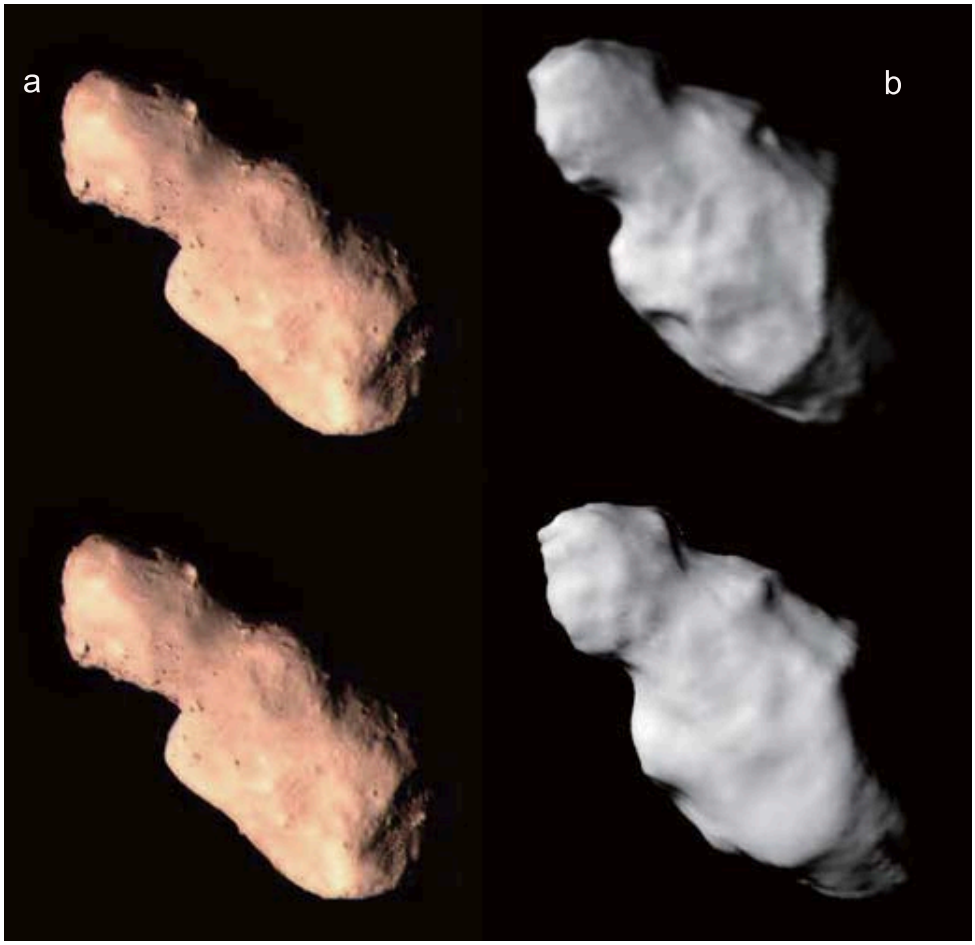

Figure 2 (a)The left panels show the optical images. (b) The right panels are the matching results of radar models, where the upper right and bottom right are related to Busch et al.'s model and Hudson et al.'s model, respectively.